# Geometric Edge Description and Classification in Point Cloud Data with Application to 3D Object Recognition

Troels Bo Jørgensen, Anders Glent Buch and Dirk Kraft
*The Maersk Mc-Kinney Moller Institute, University of Southern Denmark, Campusvej 55, Odense, Denmark*

Keywords: Edge Detection, Object Recognition, Pose Estimation.

Abstract: This paper addresses the detection of geometric edges on 3D shapes. We investigate the use of local point cloud features and cast the edge detection problem as a learning problem. We show how supervised learning techniques can be applied to an existing shape description in terms of local feature descriptors. We apply our approach to several well-known shape descriptors. As an additional contribution, we develop a novel shape descriptor, termed *Equivalent Circumference Surface Angle Descriptor* or ECSAD, which is particularly suitable for capturing local surface properties near edges. Our proposed descriptor allows for both fast computation and fast processing by having a low dimension, while still producing highly reliable edge detections. Lastly, we use our features in a 3D object recognition application using a well-established benchmark. We show that our edge features allow for significant speedups while achieving state of the art results.

## 1 INTRODUCTION

Edge detection in general is a highly investigated topic in computer vision, mainly due to the possibility of condensing the input observations with a limited loss of information. This is beneficial also for 3D applications, e.g., point cloud enrichment (Gumhold et al., 2001) and pose estimation (Buch et al., 2013a), since it can decrease computation times. For these reasons, 3D edge detection should be fast, and it should be easy to use for general point clouds, containing noise and varying sampling densities. A 3D edge detection example is shown in Figure 1.

Several other methods have been proposed to tackled the issue, including (Gumhold et al., 2001; Guy and Medioni, 1997; Pauly et al., 2002; Pauly et al., 2003). These methods tend to rely on complex handcrafted analyses of large local neighborhoods in order to determine stable edge confidences. For this reasons they become computationally expensive.

We propose to use a staged approach to produce a simpler and faster algorithm, as done in 2D by e.g., Canny (Canny, 1986), but with very different processes since we are dealing with 3D data. We first estimate the edge direction using a local neighborhood. Then we compute our local ECSAD descriptor for describing the neighborhood, and then use the descriptor to refine the edge direction estimate. Based on this descriptor we provide two alternative methods

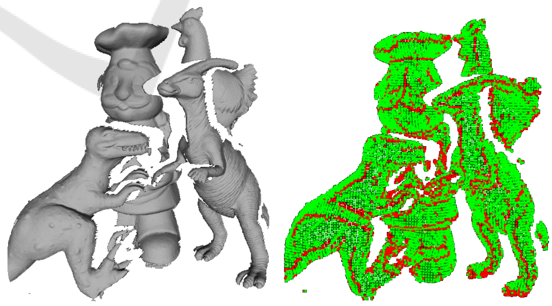

Figure 1: Left: a scene captured with a laser scanner (Mian et al., 2006). Right: edge detector response using our method (red means high confidence).

for finding an edge confidence: 1) directly using a curvature estimate produced by our descriptor or 2) using machine learning techniques with labeled training data. Finally, we adopt a non-maximum suppression technique similar to that of Canny for our 3D edges to arrive at a more condensed representation of point clouds, which is desirable for matching tasks in e.g., object recognition applications.

We evaluate both our curvature based and learning based edge detectors against several other methods on point cloud data from multiple sensor modalities. For these experiments, we have manually annotated both training and test data, which provides a benchmark for comparing 3D edge detectors, and allows for future extensions. In a final application, we apply our edge



Jørgensen T., Buch A. and Kraft D..
Geometric Edge Description and Classification in Point Cloud Data with Application to 3D Object Recognition.
DOI: 10.5220/0005196703330340
In *Proceedings of the 10th International Conference on Computer Vision Theory and Applications* (VISAPP-2015), pages 333-340
ISBN: 978-989-758-089-5

representation to a 3D object recognition and 6D pose estimation system and show how to achieve both high recognition rates and significant speedups during this process.

This paper is structured as follows. We start by relating our work to other methods for edge detection in Section 2. Then we present our descriptor which is used for reliable edge detection in Section 3. We then show in Section 4 how any descriptor can be used for learning an edge detector. In Section 5 we present a simple edge thinning scheme for point clouds. In Section 6 we provide extensive experiments of various edge detectors, and we additionally show how to use our features for 3D object recognition. Finally, we make concluding remarks in Section 7.

## 2 RELATED WORK

The majority of edge detectors have been developed for 2D images, and one of the most common edge detection algorithms is the Canny edge detector (Canny, 1986), which revolves around semi-global methods in order to capture more salient features. In (Choi et al., 2013), Canny based methods were applied to RGB-D images from a Kinect camera in order to determine geometric and color based edges in organized point clouds.

Geometric edge detection in general 3D data structures has also gained some attention. For instance, (Bähnisch et al., 2009; Monga et al., 1991) have implemented edge detector in voxel based 3D images. These methods are largely extensions of the Canny detector to 3D, with a few modification to reduce computation times.

For unorganized point clouds, local point or direction information has been exploited to detect edges. In (Guy and Medioni, 1997) a PCA analysis of the normals is made in order to determine how much the surface varies. The work in (Pauly et al., 2003) proposes to use the curvature estimates at several different scales in order to determine a edge confidence. Gumhold et al. (Gumhold et al., 2001) propose to use a more complex combination of eigenvalues, eigenvectors and other curvature estimates in order to determine a handcrafted edge confidence. This paper also proposes to use a minimum spanning tree where short branches are removed in order to do edge thinning. A final spline fitting provides a smoother visual representation.

In this work, we address the detection of 3D edges in unorganized (or unstructured) point clouds. Such edges often occur at orientation discontinuities where two planar surfaces coincide. For this task, we have derived an appropriate local shape descriptor, termed ECSAD, which can be used for detecting edges, either directly by a curvature estimate produced by the descriptor or by learning an edge classifier in descriptor space. To our knowledge, current shape descriptors, such as e.g., (Johnson and Hebert, 1999; Mian et al., 2006; Rusu et al., 2009; Tombari et al., 2010), are focused strictly on the task of describing local shape patches of arbitrary geometry for use at a later matching stage.

Finally, we motivate the use of our edges and associated descriptors in a 3D object recognition application, where we also apply our descriptor for matching, leading to state of the art recognition performance. We note that, similar to our work, the edges detected in (Buch et al., 2013a; Choi et al., 2013) were also applied for object registration, in the latter case based on point pair features, originally proposed by (Drost et al., 2010). However, the edge detection method of (Choi et al., 2013) is restricted to organized RGB-D images, and not general 3D shapes, which renders evaluations against our work impossible. We do, however, compare ourselves with the registration algorithm of (Drost et al., 2010).

## 3 LOCAL SURFACE DESCRIPTOR FOR EDGE DETECTION

We have developed a local descriptor focusing on edge detection and classification, partly to determine the direction of the edges, and partly to be used in supervised learning for edge detection. The descriptor is a vector of relative angles between opposing sides of the edge, which we have found to provide a good description for geometric edges caused by orientation discontinuities. Before descriptor estimation, the input point cloud is down-sampled to a uniform resolution. The radius of the spherical support (the area that influences the descriptor) is a free parameter, but we have consistently used a value of five times the down-sampling resolution for simplicity.

As will be explained in the following, our descriptor uses a spatial decomposition which gives each spatial bin approximately the same circumference. Contrary to other descriptors that use histograms, our uses simple but stable angle measurements. For these reasons, we term our descriptor *Equivalent Circumference Surface Angle Descriptors* (ECSAD).

**Spatial Decomposition.** Similar to other local surface descriptors, we use a spatial decomposition, which is illustrated in Figure 2 by a cross section

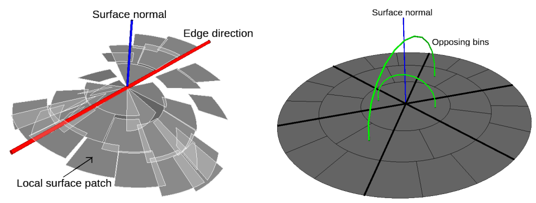


Figure 2: Left: visualization of the computed descriptor at an edge point with a tangent direction (red) and a surface normal (blue), please see text for a description how these are defined. The spatial bins are intersected by a number of surface points, and the contents of each bin is visualized by the plane patch spanned by these intersecting surface points. Right: a cross section showing the tangent plane of the local support, showing the decomposition used by our descriptor.

through the spherical region. Our descriptor splits the local space along the radial and azimuth dimensions, but not along the elevation as in e.g., (Frome et al., 2004; Tombari et al., 2010). This choice is justified by the fact that it is extremely rare that more than one surface passes through the same azimuth bin at different elevations, thus resulting in a high fraction of empty bins along the elevation. This again leads to instabilities towards position noise, and we have found this to produce worse results for edge detection and description. In Figure 2, left this can be seen as noise in the elevation of the surface patches.

Instead, we have devised a more sophisticated and uneven binning of the azimuth dimension (see Figure 2, right). We start by splitting the local space into six equiangular azimuth bins of 60° through all radial levels (bold lines). Now, for each of these six azimuth bins, we increase the number of azimuth splittings by one for each radial increment, giving a total increase of six azimuth bins per radial level (thin lines). This leads to an almost uniform angular coverage of all the bins in the azimuth dimension, and we have found this to produce much better performance than simply using an equal number of azimuth bins at all radial levels. We have tested different numbers of radial levels and found a good compromise between specificity and robustness for four radial levels (note that only three radial levels are shown in Figure 2, right).

**Reference Frame Estimation and Bin Angles.** The first step of the algorithm is to estimate the surface normal and a tangential edge direction of the center point which is to be described. This is done by the eigendecomposition of the scatter matrix of all the points in the support, giving the direction and normal along the eigenvectors corresponding to the largest and smallest eigenvalues, respectively. The local reference frame (LRF) x- and z-axis is given by these two vectors, and the y-axis by their cross product. Then we map each of the supporting points into the correct spatial bin based on its radial and azimuth coordinates relative to the center point. This is done using the direction vector from the center point to the supporting point. The radial component is immediately given by the norm of this vector, while the azimuth component is given by the relative angle between this vector and the x-axis, measured in the tangent plane of the normal vector. For each bin, we now compute the relative angle between the surface normal and the direction vector to each point in the spatial bin. This angle is then averaged over all points that fall in the same spatial bin, giving a single angle measurement per spatial bin. After the angles to the individual bins have been determined, an interpolation strategy is used to assign values to bins with missing information, i.e., bins which have no points.

The interpolation value of a bin is performed by averaging the angles of up to five neighbor bins: one at a lower radial level, two next to the bin at the same radial level, and the two closest at a higher radial level. The neighbors at the same and at the higher radial level are only used if they contain points and thereby an angle measurement. The interpolation then starts from the center and moves outwards. At the first radial level, the bin angle at a lower radial level defined as zero. This ensures a value will be assigned to every bin.

**Description Using Sum of Angles.** At an edge point, the x-axis separates two surfaces meeting at the center point. Our descriptor tries to approximate the angle between these two surfaces using the individual angle measurements of the spatial bins. To achieve this we identify opposing spatial bins, i.e., bins that have the same radial component but separated by an azimuth angle of $\pi$. We now take the sum of angles of each opposing bin pair, reducing the number of angle observations by a factor of two (green lines in Figure 2, right). Each angle sum approximates the angle between the coinciding surfaces, but this summation also makes our descriptor invariant to the sign of the x-axis, which is desirable, since this direction is ambiguous.

**Reference Frame Refinement and Curvature Estimate.** A special case occurs in concave regions, i.e., at points where the normal vector (z-axis) has an angle of less than $\pi/2$ to the two opposing surfaces. This can easily be measured by checking if the average of the sum of angles defined above is larger than $\pi$. In such cases, we negate the y- and z-axis of the LRF. Finally, we perform a refinement of the x-axis by treating the sum of angle entries as a local 2D map, where each entry equals the angle measurement weighted by the radial component. We compute the eigendecomposition of the covariance matrix of this local 2D map of weighted angle entries, and the edge direction will now be better approximated by the in-plane eigenvector of the smallest eigenvalue. We rotate the LRF around the z-axis to coincide with the updated x-axis. Using this refined RF, we now recompute all the sum of angle measurements to get a more robust descriptor.

As a side effect, the biggest eigenvalue of the local 2D map computed above provides a good estimate of the the local curvature around the edge. In Section 6 we show results of using this measure for edge detection. In all the experiments, we have used four radial levels, leading to a descriptor dimension of $(6+12+18+24)/2 = 30$

In order to use the descriptor in pose estimation, it is beneficial to orient the normals to point outwards from the underlying objects. This is done to improve correct match rates, since it enables distinction between convex and concave regions. For scenes, this is done by rotating the scene normals towards a viewpoint. For models it is done based on a technique proposed by (Hoppe et al., 1992).

If the normal signs are changed, the descriptors are updated, similarly to how concave regions are oriented to produce similar descriptors for concave and convex regions to simplified edge detection.

## 4 SUPERVISED LEARNING FOR EDGE DETECTION

Using our ECSAD descriptors, a random forest (RF) classifier (Breiman, 2001) was trained in order to determine edge confidences in point clouds containing structured noise, such as point clouds captured by range sensors.

The training dataset consists of manually labeled point clouds, captured by Kinect cameras, stereo cameras and sampled from CAD models. Examples of labeled point clouds from these different sources are seen in Figure 3. Here the red lines are positive edge examples, the blue lines are ignored due to uncertainty of the human annotator, and the rest of the points are negative examples. We trained using four CAD models, two stereo scenes, two Kinect scenes and three Kinect views of different objects. All in all this provided more than 12500 positive and 285000 negative training examples.

These data, along with the local feature descriptors computed over the full point clouds, were then used in order to train the random forests. Based on multiple runs over different parameters, we found that a point cloud resolution of 4 mm, a support radius of 20 mm, and an RF with 30 trees and a maximum tree depth of 15 provided good results. Similar figures hold for the other methods which we will compare against in Section 6.

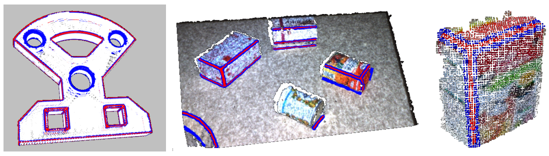

Figure 3: Examples of labeled point clouds from various sources used for training (relative sizes are not preserved in this figure). Ground truth edges (red) are used as positive examples, and transition regions between edges and non-edges (blue) are discarded during training. The rest of the points are non-edges, which are used as negative examples. Left: an ideal CAD model, resampled to a point cloud. Middle: a real scene with projected texture pattern, reconstructed by a block matching algorithm. Right: a partial view of a textured object, taken from the RGB-D Dataset (Lai et al., 2011).

In the test phase, a new point cloud with computed feature descriptors is fed to the RF classifier. The output edge confidence at a feature point is then simply given by the number of trees in the RF that classify the feature as an edge.

A smoothness technique is applied to the edge confidences, which is beneficial as an extra step before applying non-maximum edge suppression for thinning the edge map. This is simply implemented by determining the ten closest points to the edge point in question and averaging the edge confidences. After this step, the cloud is ready for non-maximum edge suppression.

## 5 EDGE THINNING

For some applications, e.g., object recognition, a sparse representation can be desirable. One of the simplest solutions in our case is to use a non-maximum edge suppression technique. This is implemented by determining the 20 closest edge points to a potential edge. Denote the current center point as $p_C$ and a neighbor as $p_N$, both with associated edge directions $d_C$ and $d_N$ and edge confidences $c(p_C)$ and $c(p_N)$. To determine whether $p_C$ suppresses $p_N$, three criteria are used. First, $p_C$ must have the highest edge confidence:

$$c(p_C) > c(p_N) \tag{1}$$

Secondly, we impose the following collinearity constraint:

$$\angle(d_C, p_N - p_C) > \frac{3}{8} \cdot \pi \tag{2}$$

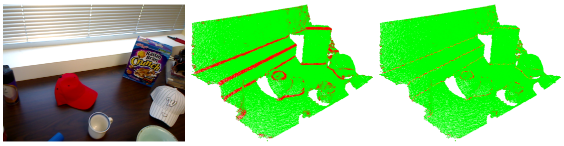

Figure 4: Left: a table scene from the RGB-D Dataset. Middle: edge detector responses. Right: remaining edges after non-maximum suppression.

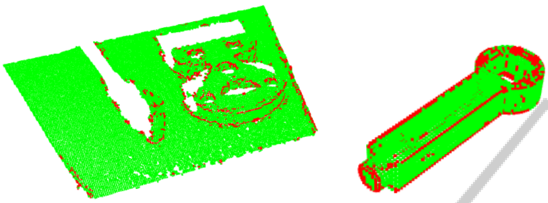

Figure 5: Edge responses after non-maximum suppression. Left: A real scene with projected texture pattern, reconstructed by a block matching algorithm. Right: An ideal CAD model resampled to a point cloud.



This ensures that points on the same line do not suppress each other. Thirdly, we require the following:

$$\angle(d_C, d_N) < \frac{\pi}{4} \tag{3}$$

This ensures that orthogonal edges do not suppress each other. As an optimization, we check (1)–(3) bidirectionally, i.e., if a neighbor point suppresses the center point, the center point is discarded. This step is done to reduce the number of neighborhood searches, which is computationally expensive in point clouds.

A visualization of this suppression process is shown for a Kinect scene in Figure 4. We note that the thinning is an optional step, and in this paper we use it only in the final object recognition application. For a fair comparison of edge detectors, it is more appropriate to directly use the output edge confidences, as we will show in Section 6.1.

Figure 1 and Figure 5 show the edge response after line thinning for three other point clouds . Here it is seen that the detector has a decent response for all data sources, but it should be noted that the response near borders is poor, partly due to higher noise levels in these areas. In the Kinect point cloud it is also seen that the responses become poor at the most distant parts of the scene, where the noise and quantization levels are particularly high.

## 6 EXPERIMENTS

In this section we provide experimental results both for our edge detection algorithms, and for an object recognition application. All algorithms were implemented in single-threaded C++ applications, primarily using functionality from the Point Cloud Library[1] (Rusu and Cousins, 2011). OpenCV[2] was used for its interface to machine learning algorithms.

The algorithms was evaluated using an Intel core i3 3217U, 1.8GHz with 4GB RAM. This computer is roughly equivalent to the one used by Drost et al. (Drost et al., 2010).

We have tested a range of parameters for our method, and the performance varies between different data sources (Kinect, CAD and stereo). A full evaluation of these parameters and their influence on the performance on various data sources is beyond the scope of this paper. In this section we present results using the previously mentioned parameter values, providing good results in general for all data sources.

### 6.1 Quantitative Evaluation of Edge Detectors

For the purpose of evaluating the strength of our edge detector, we have created test data in a similar manner to the training data (see Figure 3). The test set was generated using two CAD models, two stereo scenes and two Kinect scenes, providing more than 6000 positive and 170000 negative test examples, respectively. We split the test set into three different categories (CAD, stereo and Kinect), as we have observed quite a varying performance across the different data sources. Note that the training set has not been split; only one training pass over the full training set is performed. All training and test data are publicly available on our web site.[3]

We train an RF classifier using our ECSAD descriptor. Additionally, we perform the same procedure using two recent shape descriptors, the Signature Histogram of Orientations (SHOT) (Tombari et al., 2010) and the Fast Point Feature Histogram (FPFH) (Rusu et al., 2009). Both features have been widely used for surface description.

In addition to the RF test, we evaluate the use of the internal curvature estimate produced by our descriptor for directly providing an edge confidence. For comparison, we also include in our test other curvature estimates, namely the total surface variation (Pauly et al., 2002) (termed *Curvature*) and a multi-scale extension of this algorithm (Pauly et al., 2003) (termed *ScaleCurv*). In these two algorithms, the curvature is estimated using the three eigenvalues of the scatter matrix of the supporting points around a point,

[1] http://pointclouds.org

[2] http://opencv.org

[3] https://sites.google.com/site/andersgb1/projects/3d-edge-detection

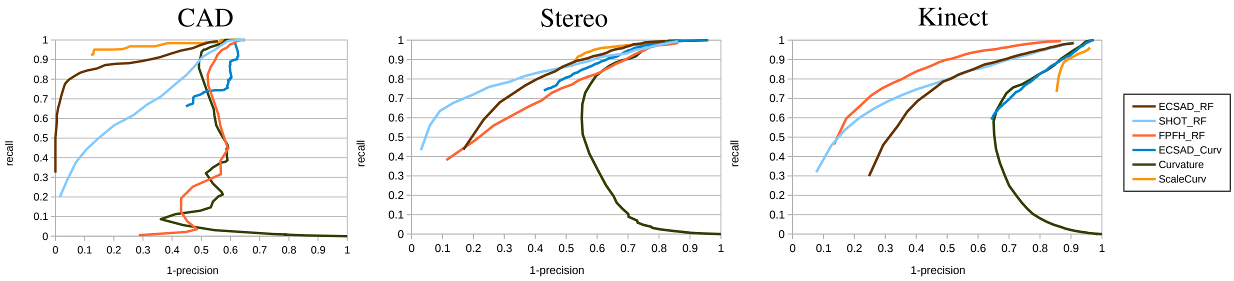


| ECSAD_RF | SHOT_RF | FPFH_RF | ECSAD_Curv | Curvature | ScaleCurv |
|---|---|---|---|---|---|
| 9.23 s | 18.17 s | 16.0 s | 7.66 s | 9.02 s | 18.8 s |

Figure 6: Performance curves in terms of (1 - precision) vs. recall for the CAD (left), stereo (middle) and Kinect (right) test scenes. The bottom table shows the accumulated detection time for all six point clouds (in total ca. 176000 points) in the test dataset. For the learned detectors, this includes both descriptor computation and RF classification.

simply by dividing the smallest eigenvalue by the sum of all three eigenvalues.

In Figure 6 we show results for all three data sources as (1 - precision) vs. recall curves, which is a standardized way to evaluate interest point detectors (Mikolajczyk and Schmid, 2005). For the ideal CAD models, which have noise-free edges, we observe a very high performance of the multi-scale curvature as edge confidence. Our learned detector comes close in performance, and shows a very high initial precision at low recall. For the real stereo and Kinect data, the performance of the curvature based detectors immediately drops, and the learned detectors become superior. For the Kinect data with the highest noise, the FPFH detector shows the best performance. Our learned detector shows comparable performance for all three data sources. In addition to this, our descriptor is computationally efficient–almost twice as fast as SHOT and FPFH. In addition, the SHOT descriptor has a dimension more than ten times higher than both FPFH and ECSAD.

## 6.2 Application: 3D Object Recognition

In order to assess the benefits of edge detection for another application, we applied a previously proposed point cloud registration algorithm to our features. The method is presented in (Buch et al., 2013b) and is based on RANSAC (Fischler and Bolles, 1981), with a crucial optimization step used for early rejection of point samples that are unlikely to produce valid pose hypotheses. We further improve the method by allowing for multiple feature matches within a predefined radius in descriptor space. The algorithm is presented below.

**Initialization:**

1. The object and scene surfaces are down-sampled to a voxel size of 3 mm to ensure a uniform point cloud resolution.
2. Edges are detected within both the object and scene point clouds using the learned RF detector, using ECSAD descriptors computed with a support radius of 15 mm. Non-maximum suppression is applied to reduce the number of features. The descriptors are stored for use below.
3. For each object edge feature, we use $k$-d trees to search for all matching feature descriptors in the scene within a radius of one unit in descriptor space.

**Iterate:**

1. Three random feature points are sampled on the object. For each of these points a random scene correspondence is retrieved from the list of correspondences generated in step 3 of the initialization.
2. Apply the pre-rejection of (Buch et al., 2013b): if any of the distances between the three object points differs more than 10 % from the equivalent distance between the corresponding scene points, continue to the next iteration.
3. A pose hypothesis is generated based on the three matches.
4. The pose is applied to the object point cloud, and we count the number of inliers supporting the pose by an Euclidean proximity threshold of 3 mm. Additionally, we require that the aligned normal vectors have a relative angle less than $\pi/3$. If the number of inliers satisfying both these conditions is higher than 15 % of the number of object points, we break out and consider the object as recognized.

The pre-rejection step makes the search for valid poses very fast, so we run the algorithm for a maximum of 100000 iterations. In case all 100000 iterations are completed without finding a pose with more than 15 % inliers, the best pose is chosen to ensure recognition of highly occluded objects. Finally the determined pose is refined by ten iterations of the iterative closest point algorithm (Besl and McKay, 1992).

As an additional test, we also implemented our method with the full set of ECSAD features at all down-sampled surface points, not only at the edge features. We have tested our algorithms on the well-known laser scanner dataset by Mian et al. (Mian et al., 2006), consisting of four complete objects to be recognized in view-based 50 test scenes.[4] For comparison, we present previous results for three state of the art methods: Spin images by Johnson and Hebert (Johnson and Hebert, 1999), Tensor matching by Mian et al. (Mian et al., 2006), and finally the PPF registration by Drost et al. (Drost et al., 2010). The results are presented as occlusion vs. recognition rate, similarly to how (Mian et al., 2006) evaluated the original algorithms on the dataset. Occlusion is the percentage of the object which is visible, and recognition rate is the relative number of times an object is recognized in the 50 scenes. An object pose is accepted if it diverges with less than 12° and 5 mm from the ground truth pose, which is similar to the criterion used in (Drost et al., 2010).

For our surface-based method, we see a high performance, which indicates a high performance of the registration algorithm. The edge features, being more discriminative, show an even higher performance, giving the best recognition results at the highest occlusion rates. Additionally, we report the average recognition time per object, which for our algorithm includes both ECSAD computation, edge detection by the classifier and non-maximum suppression. These numbers clearly show the gain of using our sparse edge representation, giving a significant speedup relative to both the surface-based registration algorithm and the fast PPF registration.

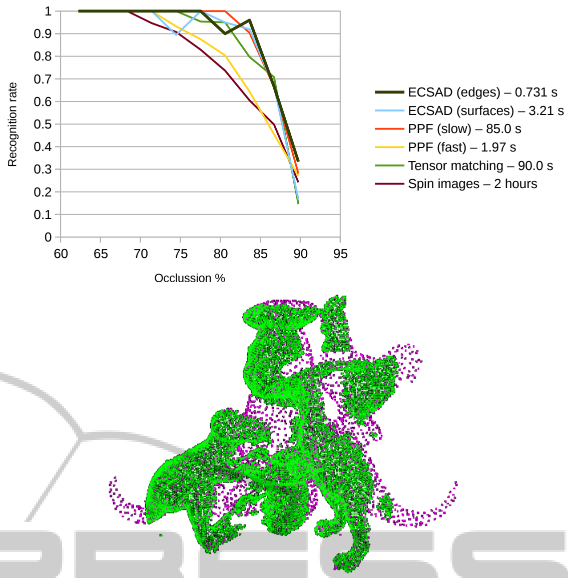


Figure 7: Comparison of our surface- and edge-based recognition systems with other works. The upper figure shows different pose estimation algorithm performances in terms of recognition-occlusion curves along with average running times per object. The bottom figure shows the first scene of the dataset, also shown in Figure 1. The magenta objects are the determined poses, so in this scene all objects have been correctly recognized.

## 7 CONCLUSION AND FUTURE WORK

A new edge detection approach for 3D point clouds from various sources has been developed, focusing on speed and overall performance. In these aspects our detector shows superior performance compared to other methods, even with limited parameter tuning.

A RANSAC based pose estimation algorithm was developed, which shows that using edges can significantly improve the runtime of 3D recognition algorithms. Furthermore the simple pose estimation application matches the performance of state of the art recognition systems on an established laser scanner benchmark, while being significantly faster.

In future work, a robustness study of the local reference frame compared with other reference frame estimation algorithms would be highly interesting. Since the descriptor has the best performance for a relatively small support radius, it would be interesting to apply the edges in higher level descriptors to determine if such an approach can result in a higher match rate for large noisy scenes. It would also be interesting to investigate the performance of the descriptor if it was used in a Hough-like voting algorithm instead of a RANSAC based approach. It is doubtful that this will increase the speed for the tested recognition dataset, but it may improve the recognition rate in more complex scenarios, where segmentation is often performed. In this context it would also be interesting to investigate if the edges can be used in a point cloud segmentation algorithm.

[4] http://www.csse.uwa.edu.au/∼ajmal/recognition.html

## ACKNOWLEDGEMENTS

The research leading to these results has received funding by The Danish Council for Strategic Research through the project Carmen and from the European Community's Seventh Framework Programme FP7/2007-2013 (Specific Programme Cooperation, Theme 3, Information and Communication Technologies) under grant agreement no. 270273, Xperience.

## REFERENCES

Bähnisch, C., Stelldinger, P., and Köthe, U. (2009). Fast and accurate 3D edge detection for surface reconstruction. In *Pattern Recognition*, pages 111–120. Springer.

Besl, P. and McKay, N. D. (1992). A method for registration of 3-d shapes. *Pattern Analysis and Machine Intelligence, IEEE Transactions on*, 14(2):239–256.

Breiman, L. (2001). Random forests. *Machine learning*, 45(1):5–32.

Buch, A. G., Jessen, J. B., Kraft, D., Savarimuthu, T. R., and Krüger, N. (2013a). Extended 3D line segments from RGB-D data for pose estimation. In *Scandinavian Conference on Image Analysis (SCIA)*, pages 54–65. Springer.

Buch, A. G., Kraft, D., Kamarainen, J.-K., Petersen, H. G., and Kruger, N. (2013b). Pose estimation using local structure-specific shape and appearance context. In *Robotics and Automation (ICRA), 2013 IEEE International Conference on*, pages 2080–2087.

Canny, J. (1986). A computational approach to edge detection. *Pattern Analysis and Machine Intelligence, IEEE Transactions on*, PAMI-8(6):679–698.

Choi, C., Trevor, A. J., and Christensen, H. I. (2013). RGB-D edge detection and edge-based registration. In *Intelligent Robots and Systems (IROS), 2013 IEEE/RSJ International Conference on*, pages 1568–1575.

Drost, B., Ulrich, M., Navab, N., and Ilic, S. (2010). Model globally, match locally: Efficient and robust 3D object recognition. In *Computer Vision and Pattern Recognition (CVPR), 2010 IEEE Conference on*, pages 998–1005.

Fischler, M. A. and Bolles, R. C. (1981). Random sample consensus: a paradigm for model fitting with applications to image analysis and automated cartography. *Communications of the ACM*, 24(6):381–395.

Frome, A., Huber, D., Kolluri, R., Bülow, T., and Malik, J. (2004). Recognizing objects in range data using regional point descriptors. In *Proceedings of the European Conference on Computer Vision (ECCV)*, pages 224–237.

Gumhold, S., Wang, X., and MacLeod, R. (2001). Feature extraction from point clouds. In *Proceedings of 10th international meshing roundtable*, pages 293–305.

Guy, G. and Medioni, G. (1997). Inference of surfaces, 3D curves, and junctions from sparse, noisy, 3D data. *Pattern Analysis and Machine Intelligence, IEEE Transactions on*, 19(11):1265–1277.

Hoppe, H., DeRose, T., Duchamp, T., McDonald, J., and Stuetzle, W. (1992). Surface reconstruction from unorganized points. In *ACM SIGGRAPH Proceedings*, pages 71–78.

Johnson, A. E. and Hebert, M. (1999). Using spin images for efficient object recognition in cluttered 3D scenes. *Pattern Analysis and Machine Intelligence, IEEE Transactions on*, 21(5):433–449.

Lai, K., Bo, L., Ren, X., and Fox, D. (2011). A large-scale hierarchical multi-view RGB-D object dataset. In *Robotics and Automation (ICRA), 2011 IEEE International Conference on*, pages 1817–1824.

Mian, A. S., Bennamoun, M., and Owens, R. (2006). Three-dimensional model-based object recognition and segmentation in cluttered scenes. *Pattern Analysis and Machine Intelligence, IEEE Transactions on*, 28(10):1584–1601.

Mikolajczyk, K. and Schmid, C. (2005). A performance evaluation of local descriptors. *Pattern Analysis and Machine Intelligence, IEEE Transactions on*, 27(10):1615–1630.

Monga, O., Deriche, R., and Rocchisani, J.-M. (1991). 3D edge detection using recursive filtering: application to scanner images. *CVGIP: Image Understanding*, 53(1):76–87.

Pauly, M., Gross, M., and Kobbelt, L. P. (2002). Efficient simplification of point-sampled surfaces. In *IEEE Conference on Visualization*, pages 163–170.

Pauly, M., Keiser, R., and Gross, M. (2003). Multi-scale feature extraction on point-sampled surfaces. *Computer Graphics Forum*, 22(3):281–289.

Rusu, R. B., Blodow, N., and Beetz, M. (2009). Fast point feature histograms (FPFH) for 3D registration. In *Robotics and Automation, 2009. ICRA'09. IEEE International Conference on*, pages 3212–3217.

Rusu, R. B. and Cousins, S. (2011). 3D is here: Point cloud library (PCL). In *Robotics and Automation (ICRA), 2011 IEEE International Conference on*, pages 1–4.

Tombari, F., Salti, S., and Di Stefano, L. (2010). Unique signatures of histograms for local surface description. In *European Conference on Computer Vision (ECCV)*, pages 356–369.